Melissa Preschan, BSc

Radial bedding of segmental linings at shield TBM driven tunnels

Master's Thesis

Submitted in fulfilment of the requirements for the degree of

Diplom-Ingenieurin

Master's programme, Geotechnical and Hydraulic Engineering

at

Graz University of Technology

Supervisors

O.Univ.-Prof. Dipl.-Ing. Dr.mont. Wulf Schubert

Dipl.-Ing. Michael Rudolf Henzinger

Institute of Rock Mechanics and Tunnelling
Graz University of Technology

Graz, September 2018

Affidavit

Ich erkläre an Eides statt, dass ich die vorliegende Arbeit selbstständig verfasst, andere als die angegebenen Quellen/Hilfsmittel nicht benutzt, und die den benutzten Quellen wörtlich und inhaltlich entnommenen Stellen als solche kenntlich gemacht habe. Das in TUGRAZonline hochgeladene Textdokument ist mit der vorliegenden Masterarbeit identisch.

I declare that I have authored this thesis independently, that I have not used other than the declared sources/resources, and that I have explicitly marked all material which has been quoted either literally or by content from the used sources. The text document uploaded to TUGRAZonline is identical to the present master‘s thesis.

Datum / Date

Unterschrift / Signature

Danksagung

Zu Beginn möchte ich mich bei meinem Diplomarbeitsbetreuer Herrn DI Michael Henzinger für seine Unterstützung bedanken. Er ist mit diesem Thema an mich herangetreten und stand mir während der Erstellung stets mit hilfreichen Tipps zur Seite.

Ein großes Dankeschön auch an meinen Professor, Herrn Wulf Schubert, der mit seiner kritischen Betrachtung und seinen konstruktiven Ratschlägen die Diplomarbeit in eine neue Richtung wies.

Mein Dank gilt auch all meinen Kollegen, mit denen ich eine tolle Studienzeit verbringen durfte. Mit einigen habe ich Freunde fürs Leben gefunden.

Mein besonderer Dank gilt auch meinen Freunden zu Hause, die immer ein offenes Ohr und positive Worte für mich haben.

Mein größter Dank gilt jedoch meinen Eltern und meinem Bruder. Sie haben mich während des Studiums immer unterstützt, mich motiviert und mir stets neue Kraft gespendet. Danke, dass ihr immer für mich da seid.

Abstract

For tunnels with shielded TBM advance an annular gap between rock mass and segmental lining is created. This gap has to be backfilled as soon as possible. The properties of the used backfill material crucially affect the load-bearing behaviour of the overall system consisting of rock mass, backfill and segmental lining. In German-speaking parts of Europe the segmental linings are often dimensioned by means of the elastic bedded frame model method. When applying this method, the lining segments are discretised as straight or curved beams, using elastic bedding springs to simulate the subsoil reaction. The spring stiffness is defined by the bedding modulus. Hence, the bedding modulus constitutes an important input parameter when dimensioning the lining segments.

In this thesis, the bedding condition for circular tunnels was investigated using numerical simulations. The study demonstrated that at present analytical approaches deliver unsatisfying results for a considerable number of calculations when compared to the numerical investigation.

Hence, a new calculation method was established. Originating on the basic formulation of the bedding modulus as the relation between stresses and the corresponding deformations ($k_r = p_i/u_r$) a closed form solution was developed. The method provides the separate consideration of the backfill layer and the rock mass. This allows the calculation of the deformations on the inner surface of the annular gap by means of common approaches. Subsequently, the bedding modulus can be determined.

A very satisfying agreement was obtained when comparing the results of the new calculation method and the numerical results. This proved the correctness of the new approach and allows a closed-form and straightforward calculation method for the determination of the radial bedding modulus.

Kurzfassung

Beim Ausbruch von Tunneln mittels Schildmaschinen entsteht herstellungsbedingt ein Ringspalt zwischen Ausbruchslaibung und Tübbingausbau, welcher mit einem geeigneten Material verfüllt werden muss. Dabei beeinflussen die Eigenschaften des verwendeten Materials das Tragverhalten des Systems Gebirge-Tübbingschale maßgeblich. Die Dimensionierung der Tübbinge erfolgt im deutschsprachigen Raum häufig unter der Verwendung des elastisch gebetteten Stabzugs. Dabei werden die einzelnen Segmente durch geradlinige oder gekrümmte Stäbe diskretisiert und das umliegende Gebirge über radiale Bettungsfedern dargestellt. Die Federsteifigkeit wird dabei mithilfe des Bettungsmoduls beschrieben. Der radiale Bettungsmodul stellt somit einen maßgebenden Parameter bei der Dimensionierung der Tübbingschalen dar.

In dieser Arbeit wurde das Bettungsverhalten von kreisrunden Tunnelbauwerken mithilfe numerischer Simulationen untersucht und den derzeitigen Bettungsansätzen gegenübergestellt. Dabei zeigte sich, dass die analytischen Bettungsansätze nur für wenige Fälle zufriedenstellende Ergebnisse liefern, was eine unwirtschaftliche Dimensionierung der Tübbingschalen zur Folge haben kann.

Auf Basis der getrennten Betrachtung von Gebirge und Verpressmaterial wurde eine neue Methode zur Berechnung des Bettungsmoduls aufgestellt. Mit diesem Ansatz können die Verformungen am Übergang zwischen Tübbing und Verpressmaterial analytisch ermittelt werden. Zunächst werden die Verschiebungsverläufe mittels bereits bekannter Formelwerke berechnet. Anschließend kann mit der allgemeinen Definition des Bettungsmoduls als Verhältnis zwischen Spannung und zugehöriger Verformung (k_r=p_i/u_r), dieser mithilfe der berechneten Verformungen ermittelt werden.

Die Gegenüberstellung der analytischen und numerischen Ergebnisse zeigte eine äußerst zufriedenstellende Übereinstimmung und bestätigte folglich die Richtigkeit der neuen Berechnungsmethode. Somit ist eine direkte Berechnung des radialen Bettungsmoduls möglich.

Contents

List of Figures

List of Tables

Symbols

Roman letters

c	.....	cohesion in MPa
d	.....	tunnel diameter in m
d_1	.....	annular gap width in m
d_2	.....	influence depth of rock mass in m
E	.....	Young's modulus in MPa
E_{ag}	.....	Young's modulus of the backfill material in MPa
E_{rm}	.....	Young's modulus of the rock mass in MPa
E_s	.....	stiffness modulus in MPa
$E_{s,ag}$	.....	stiffness modulus of the backfill material in MPa
$E_{s,rm}$	.....	stiffness modulus of the rock mass in MPa
f	.....	correction factor for the evaluation of the bedding modulus in -
G	.....	shear modulus in MPa
h	.....	overburden high on the crown in m
K_0	.....	lateral pressure coefficient in -
k	.....	passive lateral pressure coefficient in -
k_r	.....	bedding modulus in MPa/m
k_ψ	.....	loosening factor in -
n	.....	control variable in -
p_0	.....	primary stress in MPa
p_a	.....	external pressure in MPa
p_i	.....	internal pressure in MPa
$p_{i,rm}$	.....	effective support pressure in MPa
Δp_i	.....	incremental internal pressure in MPa
r	.....	control variable in m
r_0	.....	tunnel radius in m

r_i	.....	inner radius of the annular gap in m
r_i	.....	inner radius of the annular gap in m
r_p	.....	plastic radius in m
u_r	.....	radial displacements in m
$u_{r,ag}$	.....	radial displacements of the annular gap in m
$u_{r,rm}$	.....	radial displacements of the rock mass in m
Δu_r	.....	incremental radial displacements in m

Greek letters

φ	.....	friction angle in °
ψ	.....	dilation angle in °
ρ	.....	density in kg $\cdot$ $10^6/m^3$
σ	.....	stress in MPa
σ_r	.....	radial stress in MPa
σ_t	.....	tensile strength in MPa
σ_{UCS}	.....	Unconfined compressive strength in MPa
ϵ_z	.....	lateral strain in -
ν	.....	Poisson's ratio in -
ν_{ag}	.....	Poisson's ratio of the backfill material in -
ν_{rm}	.....	Poisson's ratio of the rock mass in -

1 Introduction

For single or double shield TBM driven tunnels, segmental linings are frequently used as support. The segmental lining is installed within the protection of the shield. In order to allow curved alignments and to reduce frictional forces, the shield is smaller than the cutterhead and also may be designed conical. The herewith caused gap between rock mass and shield is termed steering gap. The size of the steering gap is governed by the required curve radius and the rock deformations, since they might lead to a jamming of the TBM. Since the lining segments are assembled within the shield, the gap between segments and rock mass is larger than between rock mass and shield. In order to enable a sufficient load-bearing behaviour the annular gap is filled as soon as possible. Once established, the bedding transfers the stresses between segmental linings and the rock mass. The used material crucially affects the stress redistribution behaviour. For TBMs in hard rock pea gravel, a fine-grained and closely-graded gravel, is pneumatically injected. The pea gravel exhibits a very low stiffness compared to the rock mass, and therefore, plays a decisive role for the bedding conditions.

In German-speaking parts of Europe the segmental linings are usually designed numerically using 2D continuum models or analytically by means of the so-called elastic bedded frame model method. When dimensioning using the bedded frame model method the bedding modulus represents one of the most important input parameters. The bedding modulus is not only affected by the surrounding subsoil or rock mass parameters, but also takes tunnel geometry as well as ground pressure into account. Consequently, a proper determination of the bedding modulus is often unfeasible. For a circular tunnel cross-section analytical approaches are adopted from soft ground conditions. Accordingly, the dimensioning of the segmental lining is subject to a considerable number of simplifications. Hence, the lack of more detailed approaches might lead to an uneconomic design.

2 State of the Art

When dimensioning using bedded frame model methods, the segmental lining is discretised as straight or curved elements, using elastic bedding springs to simulate the subsoil reaction (see Figure 2.1).

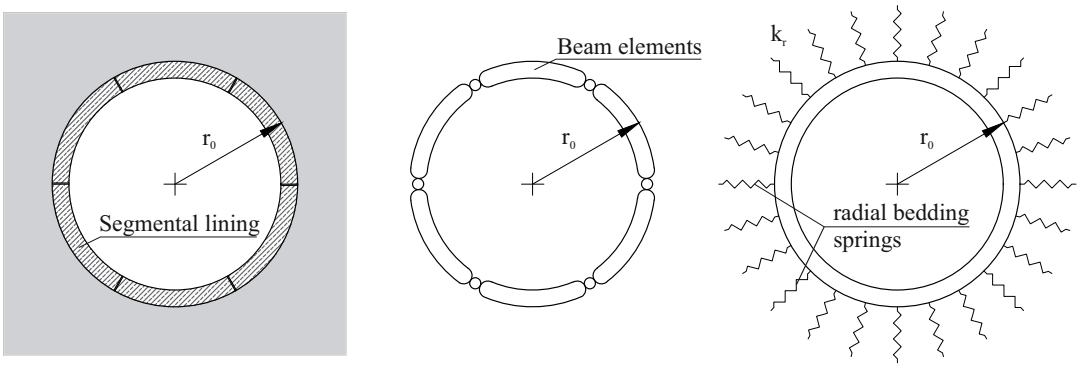

Figure 2.1: Discretisation of tunnel lining segments and surrounding subsoil.

This calculation procedure relates to the subgrade reaction method, which applies the bedding modulus k to describe the relation between bedding stresses and deformations ($\sigma = k \cdot u$).

In case of the dimensioning of segmental linings the radial bedding k_r constitutes the relation between radial bedding stresses σ_r and corresponding radial deformations u_r at the interface between subsoil and frame and is expressed as follows:

$$k_r = \frac{\sigma_r}{u_r} \tag{2.1}$$

Therefore, the bedding modulus can be calculated if the bedding stresses σ_r and the deformations u_r are known. Originating on "Theory of the Pierced Plate" the determination of these parameters is enabled under the consideration of following assumptions:

- Homogeneous, isotropic and infinite plate
- Primary stress disregarded

- Lateral pressure coefficient K_0 equals 1.0
- Plane strain conditions ($\epsilon_z = 0$)
- Linear-elastic material behaviour
- Constant internal pressure distribution along the circumferential direction

Figure 2.2 shows the Model of the Pierced Plate. The internal pressure p_i is applied on the interior edge of the plate and creates an expansion of the tunnel radius r_0, since primary stress-free conditions are assumed.

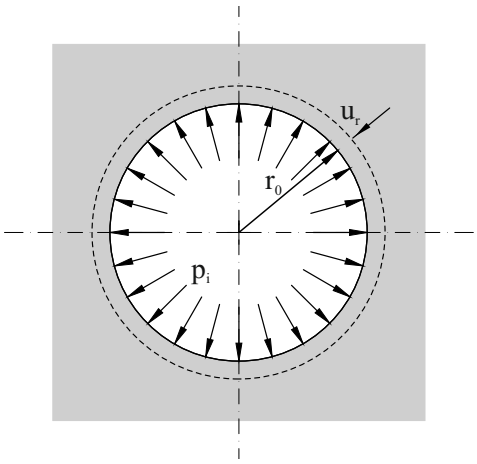

Figure 2.2: Model of the Elastic Pierced Plate.

Lamé (1852) derived a closed-form solution for the Elastic Pierced Plate. For the given problem a simplification of the original approach, which has been taken from Seeber (1999) is applied:

$$u_r = \frac{p_i \cdot r_0}{E} \cdot (1 + \nu) \tag{2.2}$$

where:
- u_r ..... radial displacements [m]
- p_i ..... internal pressure [MPa]
- r_0 ..... tunnel radius [m]
- E ..... Young's modulus [MPa]
- ν ..... Poisson's ratio [-]

Equation 2.2 considers outward facing deformations positive.

In that case the relation between the radial internal pressure p_i and the respective deformation u_r defines the radial bedding modulus k_r.

$$k_r = \frac{p_i}{u_r} \tag{2.3}$$

where: k_r ..... bedding modulus [MPa/m]
u_r ..... radial displacements [m]
p_i ..... internal pressure [MPa]

By substituting u_r of Equation 2.2 using the expression of Equation 2.3, Equation 2.4 can be provided:

$$k_r = \frac{E}{r_0} \cdot \frac{1}{1+\nu} \tag{2.4}$$

Implementing the relation between Young's modulus E and stiffness modulus E_s (Equation 2.6) delivers the alternative:

$$k_r = \frac{E_s}{r_0} \cdot \frac{1-2\nu}{1-\nu} \tag{2.5}$$

$$E_s = E \cdot \frac{1-\nu}{(1+\nu)(1-2\nu)} \tag{2.6}$$

It is apparent that the deformational behaviour of the rock mass governs the bedding modulus. However, it has to be kept in mind that additionally to the assumptions regarding the "Theory of the Pierced Plate", further simplifications apply:

- Backfill layer not implemented
- Shear bond between the rock mass and lining segments not implemented
- Mechanical properties and geometry of lining segments not considered

Due to the numerous assumptions a simplified calculation approach, which considers a correction factor f, has been established in practical applications:

$$k_r = f \cdot \frac{E_s}{r_0} \tag{2.7}$$

where: k_r ..... bedding modulus [MPa/m]
f ..... correction factor [-]
E_s ..... stiffness modulus [MPa]
r_0 ..... tunnel radius [m]

By examining Equation 2.5 it appears that f theoretically must be smaller than 1.0. In order to cover the various influencing factors and to guarantee that the bedding modulus is on the safe side, the parameter f is estimated. A wide range of recommendations for the correction factor f can be found in literature. In 1964 values between $f = 2/3$ to $f = 3.0$

were suggested as initial recommendations by Duddeck & Schulze (1964). Windels (1966) suggested values between $f = 1.0$ to $f = 1.5$. Wissmann (1968) evaluated the bedding modulus using a different methodology. With an equally loaded and infinite stripe surface he obtained a correction factor $f \approx 1.0$, which correlates to recommendations derived from the pierced plate.

In 1980 the German EBT recommendations (Duddeck, 1980) have determined following values:

$$\text{for shallow tunnels } (h < 2d): \qquad f = 1.0 \tag{2.8}$$

$$\text{for deep tunnels } (h > 3d): \qquad f = 0.5 \tag{2.9}$$

where d is the tunnel diameter and h the overburden height on the crown. In spite of the numerous recommendations the application of $f = 1$ has become common practice (Behnen et al., 2013) and the bedding modulus is calculated with:

$$k_r = \frac{E_s}{r_0} \tag{2.10}$$

In order to capture the influence of a backfill layer, Equation 2.10 has to be reformulated since it is only applicable if the backfill material exhibits an equal or higher stiffness modulus than the surrounding subsoil. The modified approach is based on two consecutive layers with constant thickness. Thus, the bedding modulus is based on the composed deformations:

$$k_r = \frac{p_i}{u_{ag} + u_{rm}} \tag{2.11}$$

where:
- k_r ..... bedding modulus [MPa/m]
- p_i ..... internal pressure [MPa]
- u_{ag} ..... radial displacements of the annular gap [m]
- u_{rm} ..... radial displacements of the rock mass [m]

The deformations are calculated:

$$u_r = u_{ag} + u_{rm} = \frac{p_i \cdot d_1}{E_{s,ag}} + \frac{p_i \cdot d_2}{E_{s,rm}} \tag{2.12}$$

By substituting u_{ag} and u_{rm} in Equation 2.11 with 2.12 the "Extended approach" (Equation 2.13) is given:

$$k_r = \frac{1}{\frac{d_1}{E_{s,ag}} + \frac{d_2}{E_{s,rm}}} \tag{2.13}$$

where:	k_r	.....	bedding modulus [MPa/m]
	d_1	.....	annular gap width [m]
	d_2	.....	influence depth of rock mass [m]
	$E_{s,ag}$	.....	stiffness modulus of the backfill material [MPa]
	$E_{s,rm}$	.....	stiffness modulus of the rock mass [MPa]

Figure 2.3 shows the principle of the "Extended approach" with consecutive layers.

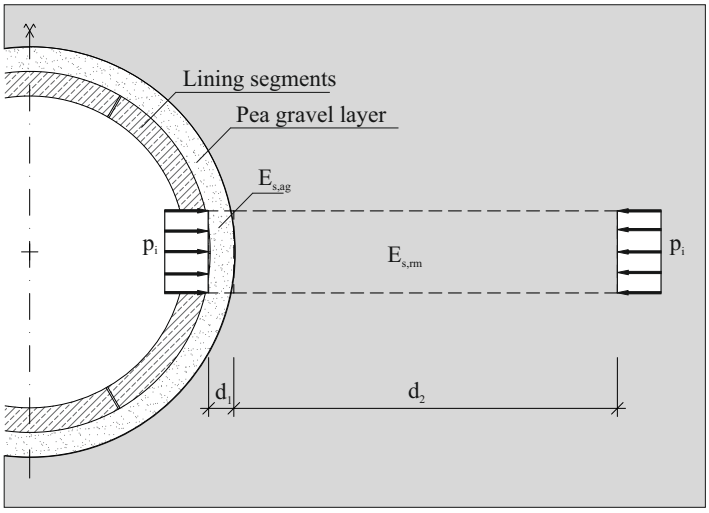

Figure 2.3: Principal of consecutive layers.

The influence depth d_2 has to be estimated. Literature provides values for d_2 between one and two times the excavation radius (Behnen et al., 2013). Thienert & Pulsfort (2011) suggest an influence depth of approximately one radius using the following equation:

$$d_2 = r_0 - d_1. \tag{2.14}$$

Under hard rock conditions, where the stiffness modulus of the rock mass $E_{s,rm}$ significantly exceeds the stiffness modulus of the backfill material $E_{s,ag}$, the bedding is primarily affected by the backfill material (Behnen et al., 2013). Thus, Equation 2.13 reduces to:

$$k_r = \frac{E_{s,ag}}{d_1} \tag{2.15}$$

where:	k_r	.....	bedding modulus [MPa/m]
	d_1	.....	annular gap width [m]
	$E_{s,ag}$	.....	stiffness modulus of the backfill material [MPa]

3 Definition of Objectives

At present, the design methodology for the segmental lining using the bedded frame model method is subject to a number of simplifications. When using the "Extended approach" incorporating the backfill layer, the influence depth of the rock mass has to be estimated, primary stress conditions are disregarded and the materials are assumed to behave linear elastically. This only represents a selection of simplification measures which have been introduced for the formulation of the current applied approaches. Their influence, however, is not sufficiently explored. Nevertheless, these approaches form the basis of the dimensioning of the segmental linings. Consequently, an improved approach (including the mechanical properties of the backfill layer and the rock mass, as well as annular gap width, tunnel radius and primary stress conditions) could provide a more appropriate dimensioning.

This work focuses on the bedding conditions within hard rock conditions using pea gravel as backfill material. The objective is the investigation of the influencing parameters on the bedding modulus by means of numerical methods. Accordingly, the incorporation of all influencing factors in the calculation methodology is targeted. Hence, a new analytical calculation method for the bedding modulus shall be introduced and confirmed by the numerical simulations.

4 Methodology

Following steps were performed to reach the previously stated aims:

- Establishment of a numerical model based on the elastic pierced plate.
- Verification of the numerical model using simple analytical approaches.
- Investigation of the bedding modulus incorporating the pea gravel layer.
- Development of a closed form solution for the determination of the bedding modulus.

The numerical study was carried out using the software FLAC3D (Itasca Consulting Group Inc., 2017). The evaluation and post processing of the numerical output was executed using MATLAB (MathWorks Inc., 2017).

4.1 Numerical model setup and post processing

The numerical model represents a pierced plate. A circular tunnel was located in the center of the model. Since the system is symmetric, a vertical plane of symmetry was introduced to reduce the computing effort.

In order to minimise the influence of the external boundary conditions and therefore to increase the reliability of the model two methods were adopted. The horizontal and vertical expansion factor was set in a range between 30 to 50 times the tunnel radius r_0, which represents a very conservative value. Additionally an external force boundary condition, which corresponds to the actual primary stress state, was applied. This guarantees small displacements at the external boundaries and results in a more accurate rock mass behaviour. The symmetry axis of the overall system, as well as the longitudinal direction were fixed in the horizontal direction with a stiff boundary. Figure 4.1 shows the numerical models. The left Figure illustrates the overall system including the external boundary conditions. The Figure

in the center and the right Figure show the models without and with the incorporation of the backfill layer.

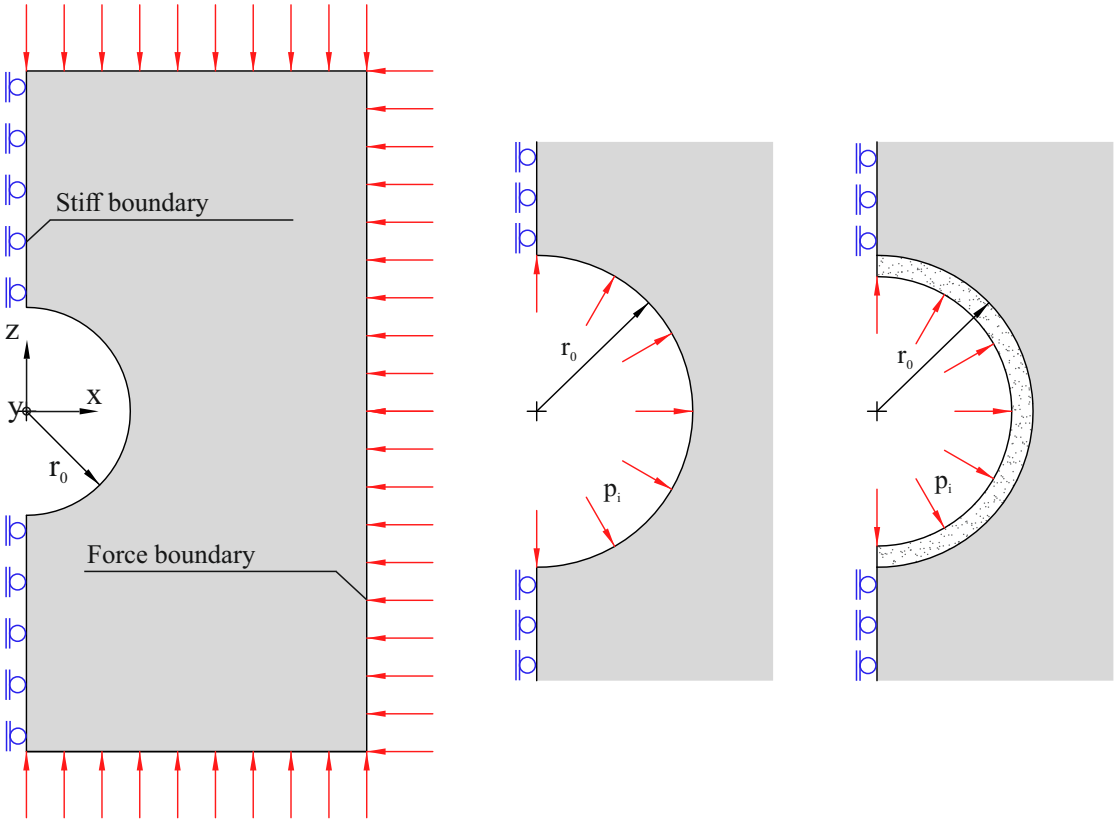

Figure 4.1: Left: Overall system of the numerical model with boundary conditions, middle: model without pea gravel, right: model incorporating the pea gravel layer

Table 4.1 describes the constitutive models, which were applied for the given tasks.

Table 4.1: Constitutive models

Material	Constitutive Model	Description	Input parameters
Rock mass	Mohr-Coulomb	Mohr-Coulomb failure criterion with tension cutoff, linear elastic stress-strain relationship and perfect plasticity	$\varphi, c, \psi, \sigma_t, E, \nu$
Pea gravel	Linear-Elastic	linear elastic stress-strain relationship	E, ν

The tunnel support was simulated as internal pressure p_i varying from 1.0 to 0.0 MPa, which

was applied at the excavation boundary. The internal pressure was applied in ten loadsteps.

The numerical simulation procedure is listed below:

1. Initializing the primary stress state and zeroing the deformations.
2. Excavation of the cavity and simultaneous application of the internal pressure of 1 MPa at the excavation boundary reaching equilibrium.
3. Stepwise decrease of the applied internal pressure reaching equilibrium after each loadstep.

The progressive plastification at the excavation boundary required decreasing loading conditions. A full relaxation without support pressure at the beginning of the numerical investigation also causes the largest deformations during this step. Consequently, the largest plastic area is formed with an internal pressure of 0 MPa. Due to the fact that plastification is irreversible, the numerical investigation delivers unreliable results for the subsequent calculations. Hence, the decrease of the internal loading in order to capture realistic results is inevitable.

The evaluation of the bedding modulus was performed using the incremental deformations between the loadsteps with their corresponding incremental internal pressure Δp_i of 0.1 MPa. This allows the consideration of nonlinear displacement development under plastified rock mass conditions. Accordingly, the bedding modulus was calculated using the secant modulus:

$$k_r = f(p_i) = \frac{\Delta p_i}{\Delta u_r} \tag{4.1}$$

$$\Delta p_i = p_i(n+1) - p_i(n) \tag{4.2}$$

$$\Delta u_r = f(p_i) = u_r(n+1) - u_r(n) \tag{4.3}$$

4.2 Verification of the numerical model using simple analytical approaches without a backfill layer

The numerical input was verified using the simplified model, which disregards the backfill layer. A primary stress-free condition was assumed ($p_0 = 0$) and the internal pressure was

applied directly on the excavation boundary. To incorporate the rock mass the constitutive model "Mohr-Coulomb" and the parameter set from Table 4.2 were used. The bedding modulus was evaluated by inserting the obtained displacements in Equation 4.1.

Table 4.2: Material parameters for Verification

Property	Symbol	Unit	Value
Density	ρ	kg $\cdot 10^6/m^3$	0.0027
Young's modulus	E	MPa	10000
Poisson's ratio	ν	-	0.25
Friction angle	φ	°	35
Cohesion	c	MPa	5
Tensile strength	σ_t	MPa	100
Dilation angle	ψ	°	0
Lateral pressure coefficient	K_0	-	1

The comparison of the numerical and analytical results proved the applicability of the numerical model. Analytical deformations were calculated using Equation 4.4 (Lamé, 1852). This approach is based on the Theory of the Elastic Pierced Plate. The sign convention determines inward facing deformations as positive.

$$u_r = (p_0 - p_i) \cdot \frac{r_0}{E} \cdot (1 + \nu) \tag{4.4}$$

In addition, the simulation was performed with a primary stress state. The results correlated when using the equation of Lamé (1852) (Equation 4.4) for elastic rock mass conditions and Equation 4.5 (Salençon, 1969) for plastified rock mass.

Salençon assumes a cylindrical cavity in an infinite medium. The body forces are disregarded, an isotropic and homogeneous material is assumed and the yield criterion is based on the Mohr-Coulomb failure criterion (Salençon, 1966, 1969). These assumptions correspond to the established numerical model. Within the plastic zone a loosening of the rock mass is taken into account. This is considered by the loosening factor k_ψ, which is governed by the dilation angle ψ. A possible softening of the rock mass within the plastic zone remains disregarded. It must be considered that this approach is inapplicable for a displacement evaluation under elastic rock mass conditions.

$$u_r = \frac{r}{2G} \cdot X \tag{4.5}$$

with:

$$
\begin{aligned}
X = {} & (2\nu - 1)\left(p_0 + \frac{\sigma_{UCS}}{k-1}\right) + \\
& + \left(\frac{(1-\nu)\cdot(k^2-1)}{k+k_\psi}\right)\left(p_i + \frac{\sigma_{UCS}}{k-1}\right)\left(\frac{r_p}{r_o}\right)^{(k-1)}\left(\frac{r_p}{r}\right)^{(k_\psi+1)} + \\
& + \left((1-\nu)\frac{(k_\psi \cdot k + 1)}{k+k_\psi} - \nu\right)\left(p_i + \frac{\sigma_{UCS}}{k-1}\right)\left(\frac{r}{r_o}\right)^{(k-1)}
\end{aligned}
\tag{4.6}
$$

where:

G	.....	shear modulus [MPa]
k	.....	passive lateral pressure coefficient [-]
k_ψ	.....	loosening factor [-]
p_0	.....	primary stress [MPa]
p_i	.....	internal pressure [MPa]
r	.....	control variable [m]
r_0	.....	tunnel radius [m]
r_p	.....	plastic radius [m]
u_r	.....	radial displacements [m]
ν	.....	Poisson's ratio [-]
σ_{UCS}	.....	Unconfined compressive strength [MPa]

Figure 4.2 shows the comparison of the numerical and analytical results. The bedding modulus is depicted on the ordinate, whereas the ordinate shows the applied internal pressure. Three different primary stress conditions are presented. The blue circles show an excellent agreement of the numerical and analytical results under elastic rock mass conditions. As can be seen under plastified conditions (red triangles and green squares) a minor discrepancy between the solutions can be identified. This is due to the limitations of the numerical model. Figure 4.3 illustrates the material state, which was obtained for a lateral pressure coefficient of 1.0. The red-colored elements represent the plastified area. As can be seen a non-uniform distribution of the plastification occurs. This is caused by the mesh, which shows varying zone depths of the single elements along the circumferential direction. Consequently, this slightly affects the resulting deformations.

Despite these drawbacks the numerical calculations delivered appropriate results and the deviations were not significant. Hence, the applicability of the numerical model was verified for various primary stress conditions.

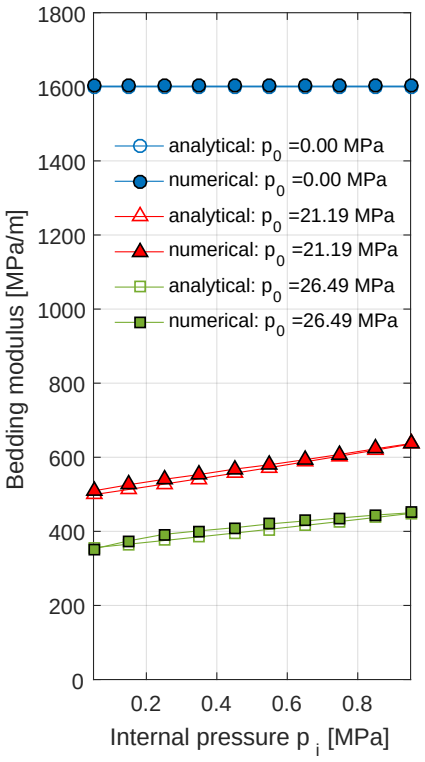

Figure 4.2: Comparison between the numerical and analytical solution.

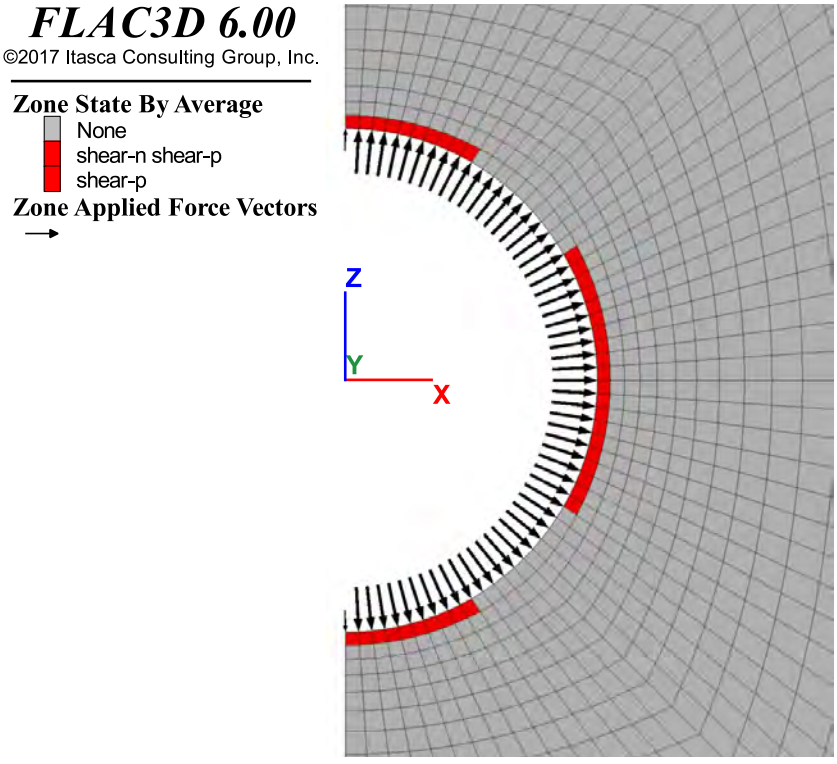

Figure 4.3: Numerical model showing a non-uniform distribution of plastification for a lateral pressure coefficient K_0 equal 1.0.

4.3 Investigation of the radial bedding modulus incorporating a backfill layer using at present analytical approaches

The influence of pea gravel on the bedding modulus was investigated using the numerical model, which incorporates the backfill layer at the interior excavation boundary. The internal pressure was applied on the interior surface of the annular gap. The bedding reaction is governed by the geometry of the tunnel as well as the annular gap, their material properties, support pressure and primary stress state. In order to obtain a representative set of numerical calculations the mechanical material properties were varied as listed in Table 4.3. In order to prevent the rock mass failing in tension, which may occur due to the internal pressure p_i for shallow tunnels, a high tensile strength σ_t of 100 MPa was assumed.

Table 4.3: Variation of the mechanical material properties

Material	Property	Symbol	Value	Unit
Rock mass	Young's modulus	E_{rm}	1000 - 100000	MPa
	Poisson's ratio	ν_{rm}	0.2 - 0.4	-
	Friction angle	φ	10 - 35	°
	Cohesion	c	5.0 - 15.0	MPa
	Tensile strength	σ_t	100	MPa
	Dilation angle	ψ	0	°
Pea gravel	Young's modulus	E_{ag}	30 - 150	MPa
	Poisson's ratio	ν_{ag}	0.2 - 0.25	-

The numerical study indicated distinct differences in the deformational behaviour between elastic and plastified rock mass as expected. Table 4.4 lists the varied parameters and their qualitative influence. It appears that the bedding reaction with elastic rock mass conditions is governed by the geometry of the tunnel, the annular gap width, as well as by the elastic properties. In contrast, with plastified conditions all investigated parameters affect the bedding reaction.

Table 4.4: Investigated parameters and their influence on the bedding modulus

Parameter	Elastic rock mass	Plastified rock mass
Tunnel radius	x	x
Annular gap width	x	x
Primary stress	–	x
Lateral pressure coefficient	–	x
Internal pressure	–	x
Elastic properties of rock mass and pea gravel	x	x
Strength properties of rock mass	–	x

x ... bedding reaction affected

– ... bedding reaction not affected

4.4 Results and discussion on performed investigations

Figures 4.4 and 4.5 illustrate the results of two selected calculations compared to the analytical approaches. The analytical results were calculated using the "Extended approach" (Equation 2.13) with $d_2 = r_0 - d_1$ (Thienert & Pulsfort, 2011) and Equation 2.15 (Behnen et al., 2013). The abscissas shows the applied internal pressure p_i, the bedding modulus k_r is depicted on the ordinate. With elastic rock mass conditions a good agreement between the numerical and analytical solutions was reached (Figure 4.4). Correlating results were obtained for a pea gravel of low stiffness within a stiff rock mass. However, the accuracy of the results depends on the stiffness ratio ($E_{s,rm}/E_{s,ag}$) between the materials. Therefore, the knowledge of the limiting stiffness ratio is required in order to obtain reliable results. A quantification of this ratio is hardly feasible due to further influencing parameters, such as Poisson's ratio and geometry. In contrast to elastic rock conditions, with plastified conditions both analytical approaches deviate significantly from the numerical solutions (Figure 4.5). The comparison showed that the actual bedding resistance is lower to a considerable extend than assumed in the analytical approximations. Hence, the results demonstrate the limitations of the at present applied analytical approaches, most notably in terms of plastified rock mass conditions.

In order to illustrate the order of magnitude of the theoretical influence depth d_2, a back-analysis was performed. To back-calculate the influence depth d_2, the "Extended approach"

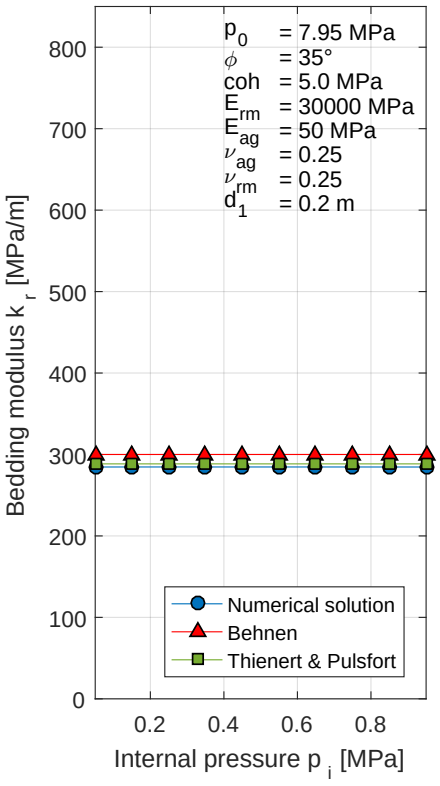

Figure 4.4: Comparison of the results showing a good agreement of numerical and analytical analysis with elastic rock mass conditions.

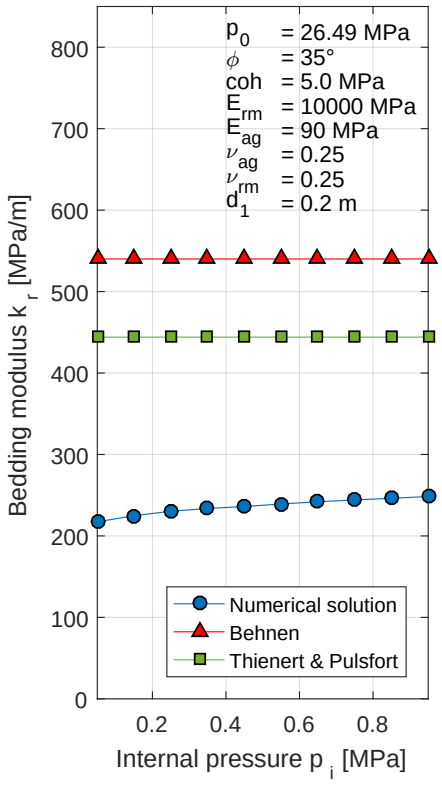

Figure 4.5: Comparison of the results showing a significant deviation of numerical and analytical analysis with plastified rock conditions.

(Equation 2.13) was used and reformulated as shown in Equation 4.7:

$$d_2 = \left(\frac{1}{k_r} - \frac{d_1}{E_{s,ag}}\right) \cdot E_{s,rm} \tag{4.7}$$

Figure 4.6 illustrates a typical development of the back-calculated normalised influence depth. For a constant stress state and a constant stiffness moduli ratio ($E_{s,rm}/E_{s,ag}$) with constant Poisson's ratios the distribution of the influence depth remains the same. A linear relationship can be identified for stiffness moduli ratios above 50 to 100. Nonlinear development appears for low ratios under plastified rock mass conditions (data not shown). The data in Figure 4.6 presents different primary stress states, whereby the blue circles show the elastic rock mass behaviour. A shift of the data upwards occurs only for plastified rock mass (red triangles and green squares).

As expected, the influence depths d_2 for stiff rock masses are lower. However, as can be seen in Figure 4.6 negative results can be obtained. This leads to the conclusion that the applied

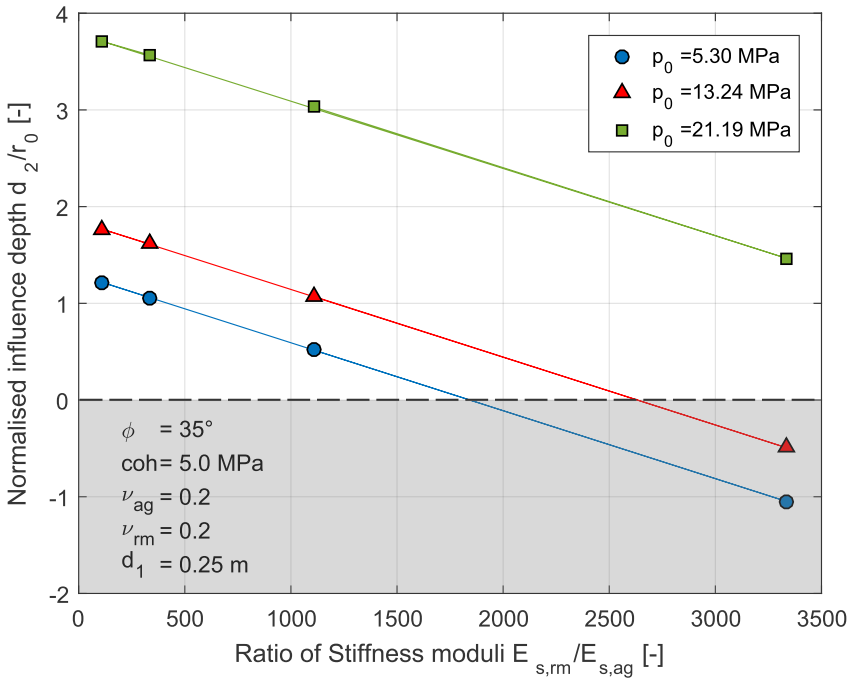

Figure 4.6: Typical development of the influence depth d_2 for different primary stress conditions.

analytical approaches are not suitable for the evaluation of the bedding modulus.

As already explained in chapter 2 the "Extended approach" (Equation 2.13) is based on two consecutive layers with constant thickness. In addition, following assumptions have been made for the formulation of this approach:

- Application of Hooke's law.
- Assumption of plain strain conditions.
- Load propagation is disregarded.

Figure 4.7 shows the principle of consecutive layers under consideration of the load propagation. Due to the circular cross section and the spatial stress condition within the materials the radial stresses decrease with increasing distance from the tunnel center. Neglecting this stress development leads to an overestimation of the radial stresses and the corresponding deformations when using the "Extended approach". Subsequently, the bedding reaction of the single layers is underestimated.

The "Extended approach" consists of two parts which describe the total deformations u_r, namely the deformations of the backfill layer u_{ag} and the deformations of the rock mass u_{rm}

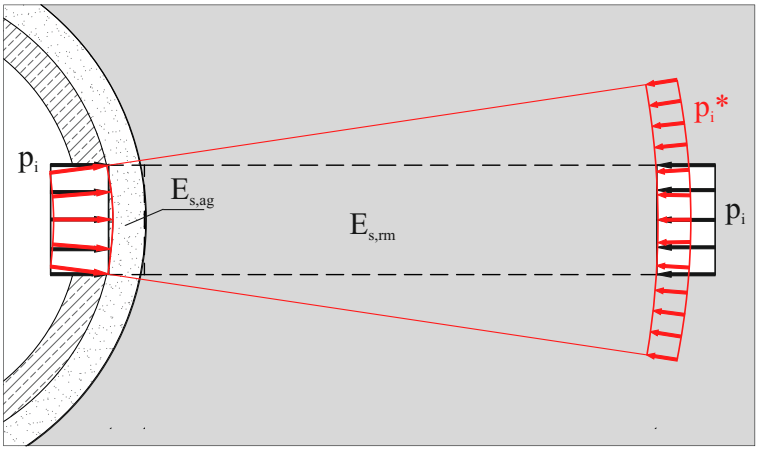

Figure 4.7: Principle of consecutive layers under consideration of the load propagation.

(see Equation 2.11). In order to obtain the analytical bedding modulus the total deformations u_r are relevant, the composition of these is not an issue. When applying the "Extended approach" the deformations of the backfill layer are calculated with the given parameters, and as explained above, overestimated. Therefore, when back-calculating the influence depth d_2 (by using the total deformations u_r, which were provided by numerical methods) the deformations of the rock mass can become negative. Consequently, negative influence depths can be obtained.

The following example demonstrates the shortcomings of the given analytical approach. The annular gap width and stiffness moduli are known, the bedding modulus was evaluated by means of numerical investigation using the general definition of the bedding modulus $k_r = p_i/u_r$.

Annular gap width:	d_1	=	0.2 m
Young's modulus of the pea gravel:	E_{ag}	=	50 MPa
Young's modulus of the rock mass:	E_{rm}	=	20 000 MPa
Bedding modulus:	k_r	=	255 MPa/m

$$k_r = \frac{1}{\frac{d_1}{E_{s,ag}} + \frac{d_2}{E_{s,rm}}} \rightarrow d_2 = \left(\frac{1}{k_r} - \frac{d_1}{E_{ag}}\right) \cdot E_{rm}$$

$$d_2 = \left(\frac{1}{255} - \frac{0.2}{50}\right) \cdot 20000 = -1.57\ [m]$$

Due to the unsatisfying results using the state of the art analytical approaches, the application of these has to be disapproved.

4.5 Establishment of a new calculation method based on displacement evaluation using familiar closed-form solutions

In this section a new calculation method is presented. The method allows the evaluation of the deformations u_r on the interior surface of the annular gap. Originating on the basic formulation of the bedding modulus (Equation 2.3) a closed-form solution can be developed. The method suggests a separate consideration of the pea gravel layer and the surrounding rock mass.

Figure 4.8 illustrates the system sketch of the new calculation method. The separate treatment of the layers allows the determination of the deformational behaviour of the pea gravel by means of the model of the thick-walled tube. The corresponding equations of the thick-walled tube were derived by Lamé (1852). When evaluating the deformations of the pea gravel the internal pressure p_i is known, the acting external stress p_a is derived under the consideration of the rock mass deformations $u_{r,rm}$. These are calculated using at present given analytical approaches. The correct assessment of the emerging radial stresses at the interface between pea gravel and rock mass ($p_a = p_{i,rm}$) is of decisive importance in order to obtain reliable results when applying this method.

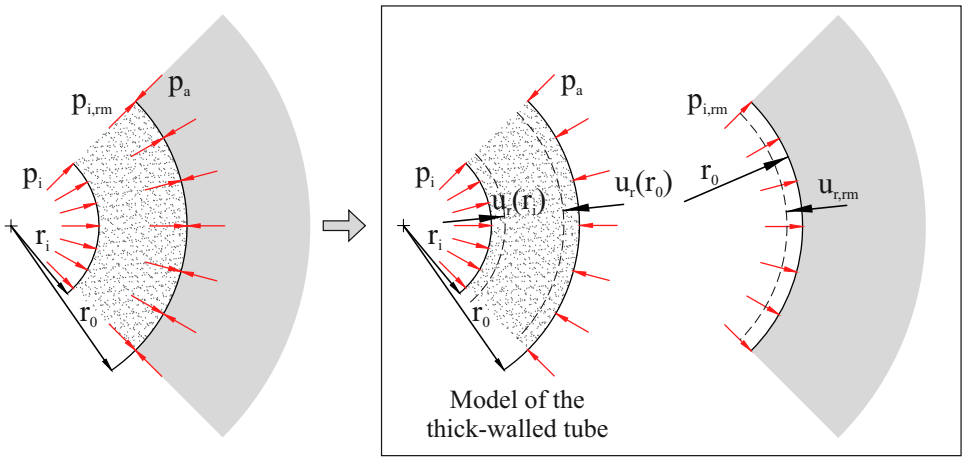

Figure 4.8: System sketch of the new calculation method for the bedding modulus.

Six calculation steps have to be undertaken for determining the bedding modulus. Figure 4.9 provides an overview:

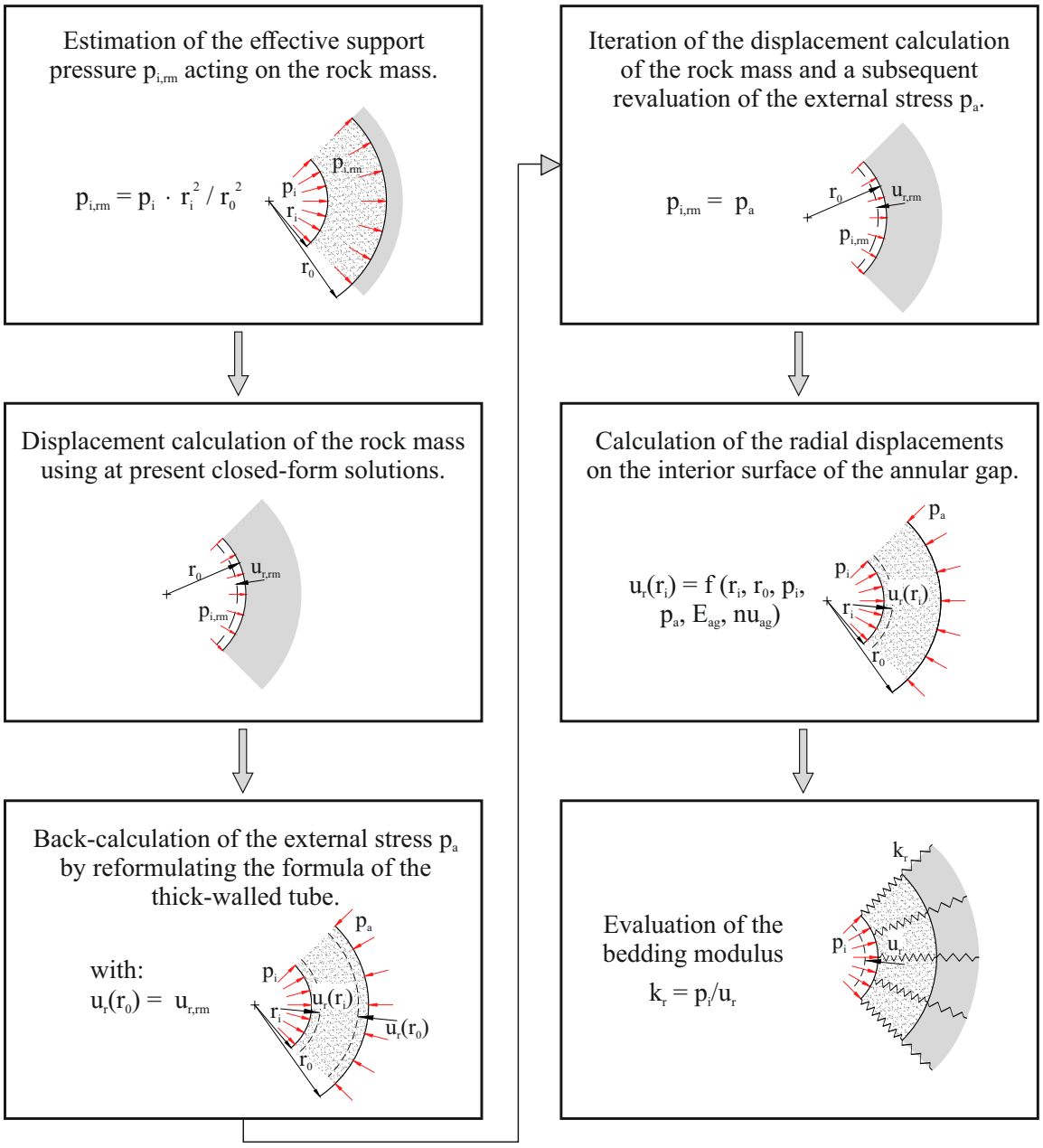

Figure 4.9: Graphical representation of the calculation steps.

4.5.1 Estimation of the effective support pressure acting on the rock mass

When considering the overall system, it is known that the internal pressure p_i is applied on the interior edge of the pea gravel layer (see Figure 4.10). Consequently, the support pressure which acts on the rock mass differs from the internal pressure. This pressure is designated as the effective support pressure $p_{i,rm}$. Initially an accurate determination of the effective support pressure is not possible, since it is governed by the interaction of rock mass and

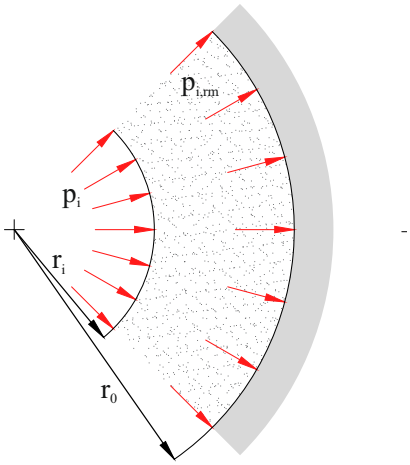

Figure 4.10: Visualisation of the interal pressure p_i and the effective support pressure $p_{i,rm}$.

backfill material. Hence, it is estimated as follows:

$$p_{i,rm} = p_i \cdot \frac{r_i^2}{r_0^2} \tag{4.8}$$

4.5.2 Calculation of the rock mass displacements

The second step is determining the rock mass deformation $u_{r,rm}$ which establishes under the effective support pressure $p_{i,rm}$ (Figure 4.11). While constituting the calculation procedure good results were obtained using Equations 4.4 (Lamé, 1852) under elastic and 4.5 (Salençon, 1969) under plastified rock mass conditions when compared to numerical investigations. Accordingly, the internal pressure p_i of the equations was substituted by the effective support pressure $p_{i,rm}$. Of course, the rock mass deformations can be evaluated using other state of the art approaches which can be found in literature (for instance such as Feder & Arwanitakis (1976)).

4.5.3 Back-calculation of the acting external stress

In the third step the model of the thick-walled tube is used (Figure 4.12). Lamé (1852) derived the corresponding equations under the consideration of a linear-elastic material behaviour. When applying this model for the given problem, plane strain conditions ($\epsilon_z = 0$) are assumed. Hence, the deformations are affected by the external stress p_a, as well as the internal pressure

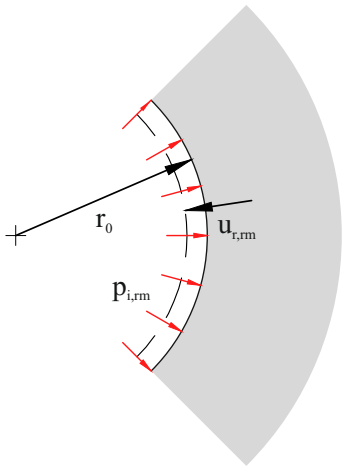

Figure 4.11: Visualisation of the rock mass model.

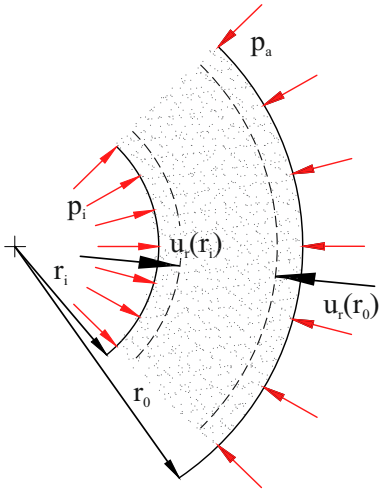

Figure 4.12: Model of the thick-walled tube.

p_i, the elastic properties and the geometry. The deformations on the exterior surface $u_r(r_0)$ can be calculated using Equation 4.9.

$$\begin{aligned} u_r(r_0) = \frac{r_0}{E_{ag} \cdot (r_0^2 - r_i^2)} \cdot [2 \cdot p_i \cdot r_i^2 \cdot (1 - \nu_{ag}^2) \\ - p_a \cdot (1 + \nu_{ag}) \cdot (1 - 2 \cdot \nu_{ag}) \cdot (1 - 2 \cdot \nu_{ag}) \cdot r_0^2 \\ + (1 + \nu_{ag}) \cdot r_i^2] \end{aligned} \tag{4.9}$$

The internal pressure, the geometry of the backfill layer, as well as the elastic material properties are known. The deformations of the exterior surface $u_r(r_0)$ are gained with the previous calculated rock mass deformations $u_{r,rm}$. The external stress p_a remains as the only unknown parameter of the equation. Hence, a reformulation of Equation 4.9 delivers a first estimation of the external stress:

$$p_a = \frac{(r_0^2 - r_i^2) \cdot E_{ag} \cdot (-u_{r,rm}) + 2 \cdot r_0 \cdot r_i^2 \cdot (\nu_{ag} - 1) \cdot (\nu_{ag} + 1) \cdot p_i}{r_0 \cdot (r_0^2 \cdot (2 \cdot \nu_{ag} - 1) - r_i^2) \cdot (\nu_{ag} + 1)} \tag{4.10}$$

While doing so, the sign convention of the thick-walled tube has to be considered:

- Positive for an expansion of the radius.
- Negative for inward facing deformations.

Therefore, the deformations $u_{r,rm}$ are considered negative for inward oriented deformations in Equation 4.10.

4.5.4 Iteration of the displacement calculation of the rock mass and revaluation of the external stress

Figure 4.13 shows the stresses, which act on the system. As can be seen, the effective support pressure $p_{i,rm}$ and the external stress p_a act both at the interface between annular gap and rock mass. Accordingly, they have to be equal in order to fulfil the criteria action equals reaction. However, the calculated external stress p_a is larger than the estimated effective support pressure $p_{i,rm}$. This follows from the fact that the previous calculations is subject to the estimation of the effective support pressure. In order to obtain the correct pressure the calculation steps two and three have to be iterated. Therefore, the effective support pressure $p_{i,rm}$ is equals the external stress p_a for the determination of the rock mass deformations.

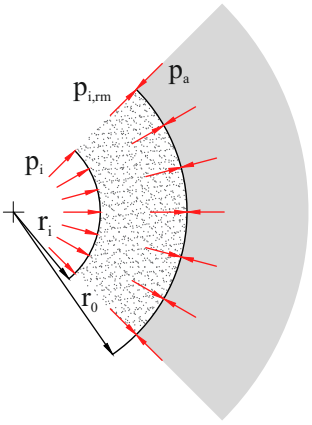

Figure 4.13: Overview of the on the system acting pressures.

4.5.5 Calculation of the radial displacements on the interior surface of the annular gap

With the assessed radial stress at the interface between pea gravel and rock mass, the deformations on the interior pea gravel surface are calculated. Therefore, the equation of the thick-walled tube is applied:

$$u_r(r_i) = \frac{r_i}{E_{ag} \cdot (r_0^2 - r_i^2)} \cdot [p_i \cdot ((1+\nu_{ag}) \cdot (1-2\cdot\nu_{ag}) \cdot r_i^2 + (1+\nu_{ag}) \cdot r_0^2) - 2 \cdot p_a \cdot r_0^2 \cdot (1-\nu_{ag}^2)] \tag{4.11}$$

4.5.6 Evaluation of the bedding modulus

Finally the evaluation of the bedding modulus is done. The calculated deformation represents the total deformation which is established in terms of the overall system consisting of rock mass and pea gravel. However, the incremental deformation which results from the pressure increase is significant. Therefore, the bedding modulus has to be calculated as the secant modulus between two stress levels. The incremental deformations $\Delta u_r(r_i)$ are implemented into the basic formulation:

$$k_r = \frac{\Delta p_i}{\Delta u_r} \tag{4.12}$$

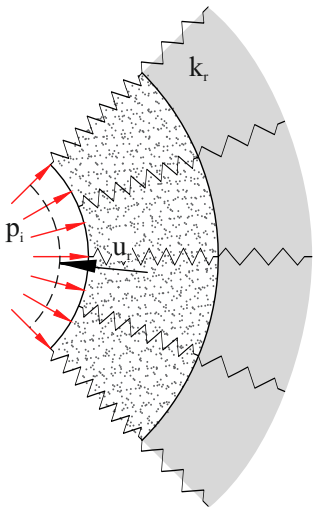

Figure 4.14: New calculation approach originated from the model of the thick-walled tube.

5 Results

In order to proof the applicability of the new calculation method a comparison of the numerical and analytical results was performed. The verification was performed using incremental internal pressures Δp_i of 0.1 MPa. For the evaluation of the radial stress at the interface between pea gravel and rock mass one iteration process proved to be sufficient. Any further iteration steps do not improve the results.

For calculations with elastic rock mass conditions an excellent agreement between numerical and analytical calculations was reached. A minor discrepancy between the solutions was identified under plastified conditions. The deviations were always below 10% for the investigated cases. However, the larger deviations occurred at the transition from elastic to plastified rock mass. This is caused by the non-uniform distribution of the plastification, which occurs due to the varying zone depths of the elements along the circumferential direction.

Figures 5.1 and 5.2 illustrate the comparison between analytical and numerical solutions. The circles indicate the numerical solution, whereas the triangles show the analytical results. Each figure presents three different calculations of varied pea gravel stiffness. The left Figure presents the results for a rock mass of poor stiffness under low stress conditions. Figure 5.2 shows the comparison for a stiff rock under high stress conditions, where plastification occurs.

The comparison verified the correctness of the new calculation method. However, it has to be considered that the application limits are subject to the approaches, which are used for the displacement calculation. Therefore, this approach is only suitable, if linear elasticity and the Mohr-Coulomb failure criterion are appropriate for describing the subsoil behaviour.

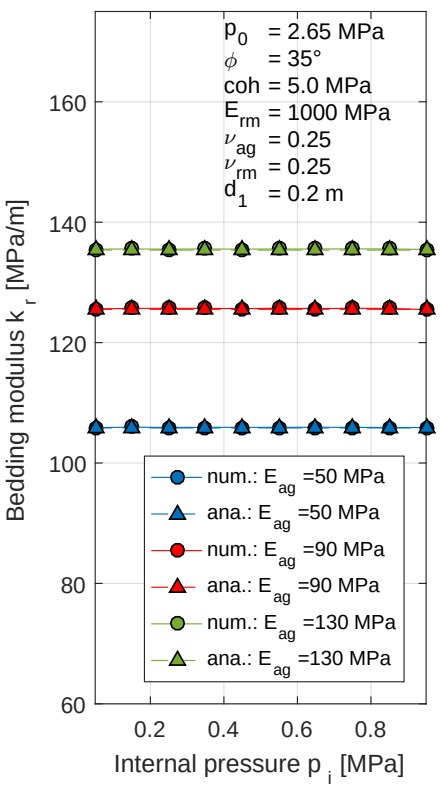

Figure 5.1: Comparison of the results showing an excellent agreement with elastic rock mass conditions.

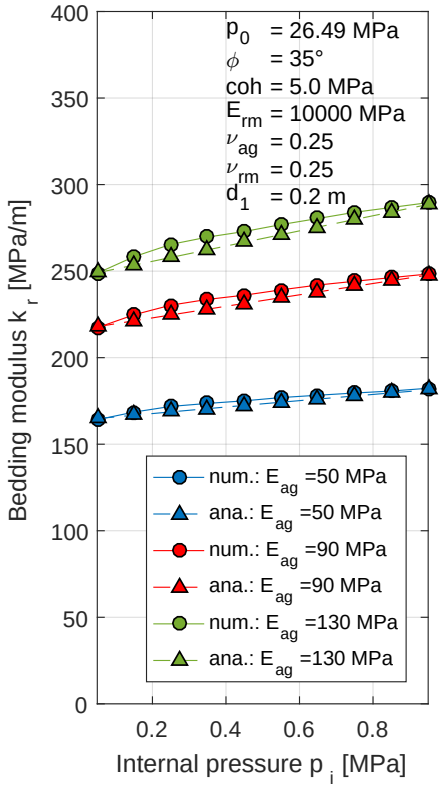

Figure 5.2: Comparison of the results showing a good agreement with plastified rock mass conditions.

6 Application Example

This example demonstrates the application of the new calculation method, which was presented in this work. Following parameters are assumed:

Tunnel geometry:

Tunnel radius:	r_0	=	5 m
Annular gap width:	d_1	=	0.20 m

Rock mass:

Primary stress:	p_0	=	21 MPa
Lateral pressure coefficient:	K_0	=	1.0
Support pressure (internal pressure):	p_i	=	0.55 MPa
Young's modulus:	E_{rm}	=	5000 MPa
Poisson's ratio:	ν_{rm}	=	0.3
Friction angle:	φ	=	35°
Cohesion:	c	=	5 MPa

Pea gravel:

Young's modulus:	E_{ag}	=	50 MPa
Poisson's ratio:	ν_{ag}	=	0.20

The inner radius of the annular gap is given as: $r_i = r_0 - d_1 = 5 - 0.2 = 4.8$ m.

In order to evaluate the secant modulus an incremental stress of 0.1 MPa is assumed. Therefore, the displacements with an internal pressure of 0.50 MPa and 0.60 MPa are calculated.

6.1 Analytical calculation of the bedding modulus

For reasons of simplicity only the calculation steps of an internal pressure of 0.50 MPa is presented. A summary of the results can be found in Table 6.1. Following steps have to be performed:

1. Estimation of the effective support pressure acting on the rock mass

In a first step the effective support pressure $p_{i,rm}$ which develops due to the assumed internal pressure p_i has to be estimated:

$$p_{i,rm} = p_i \cdot \frac{r_i^2}{r_0^2} = 0.45 \cdot \frac{4.8^2}{5.0^2} = 0.4608 \; [MPa]$$

2. Displacement calculation of the rock mass

Subsequently the rock mass deformations considering the effective support pressure is calculated. Under application of the closed-form solution of Salençon (1969), rock mass deformations $u_{r,rm}$ of 0.0306 m are obtained.

3. Back-calculation of the external stress

The back-calculation of the external stress p_a is performed using the reformulated equation of the thick-walled tube:

$$p_a = \frac{(r_0^2 - r_i^2) \cdot E_{ag} \cdot (-u_{r,rm}) + 2 \cdot r_0 \cdot r_i^2 \cdot (\nu_{ag} - 1) \cdot (\nu_{ag} + 1) \cdot p_i}{r_0 \cdot (r_0^2 \cdot (2 \cdot \nu_{ag} - 1) - r_i^2) \cdot (\nu_{ag} + 1)}$$

$$p_a = \frac{(5^2 - 4.8^2) \cdot 50 \cdot -0.0961 + 2 \cdot 5 \cdot 4.8^2 \cdot (0.2 - 1) \cdot (0.2 + 1) \cdot 0.45}{5 \cdot (5^2 \cdot (2 \cdot 0.2 - 1) - 4.8^2) \cdot (0.2 + 1)}$$

$$p_a = 0.4977 \; [MPa]$$

4. Iteration of the calculation steps two and three

The iteration of calculation steps two and three using $p_{i,rm} = p_a$ gives rock mass deformations $u_{r,rm}$ of 0.0304 m and an external stress p_a of 0.5944 MPa.

5. Calculation of the radial displacements

The evaluation of the radial displacements on the inner radius of the annular gap follows:

$$u_r(r_i) = \frac{r_i}{E_{ag} \cdot (r_0^2 - r_i^2)} \cdot [p_i \cdot ((1 + \nu_{ag}) \cdot (1 - 2 \cdot \nu_{ag}) \cdot r_i^2 + (1 + \nu_{ag}) \cdot r_0^2) - 2 \cdot p_a \cdot r_0^2 \cdot (1 - \nu_{ag}^2)]$$

$$u_r(r_i) = \frac{4.8}{50 \cdot (5^2 - 4.8^2)} \cdot [0.45 \cdot ((1 + 0.2) \cdot (1 - 2 \cdot 0.2) \cdot 4.8^2 + (1 + 0.2) \cdot 5^2) - 2 \cdot 0.4771 \cdot 5^2 \cdot (1 - 0.2^2)]$$

$$u_r(r_i) = -0.0289 \ [m]$$

The negative results indicate inward facing deformations when considering the sign convention of the applied equations.

Table 6.1 lists the results of both calculations:

Table 6.1: Application example - Results

Parameter	Symbol	$p_i = 0.50$ MPa	$p_i = 0.60$ MPa	Unit
Effective support pressure	$p_{i,rm}$	0.4608	0.5530	MPa
Rock mass deformations	$u_{r,rm}$	0.0306	0.0302	m
External stress	p_a	0.4977	0.5944	MPa
Iterated rock mass deformations	$u_{r,rm}$	0.0304	0.0301	m
Iterated external stress	p_a	0.4976	0.5944	MPa
Pea gravel deformations	p_i	-0.0289	-0.0283	m

Hence, the incremental deformations for a load increase from 0.50 MPa to 0.60 MPa can be calculated:

$$\Delta u_r = |-0.0289| - |-0.0283| = 6.9185 \ \cdot \ 10^{-4} \ [m]$$

6. Determination of the bedding modulus

The final step is the determination of the bedding modulus using the secant modulus:

$$k_r = \frac{\Delta p_i}{\Delta u_r} = \frac{0.1}{0.00069} = 145 \ [MPa/m]$$

6.2 Comparison of analytical and numerical results

The numerical incremental deformations were given with $\Delta u_{r,num.} = 7.07 \cdot 10^{-4}$ [m] for the presented example. The bedding modulus was calculated:

$$k_r = \frac{\Delta p_i}{\Delta u_r} = \frac{0.1}{0.00071} = 141 \; [MPa/m]$$

Figure 6.1 shows the comparison of the analytical and numerical solutions. For an improved presentation of the results the bedding moduli for further support pressures is shown.

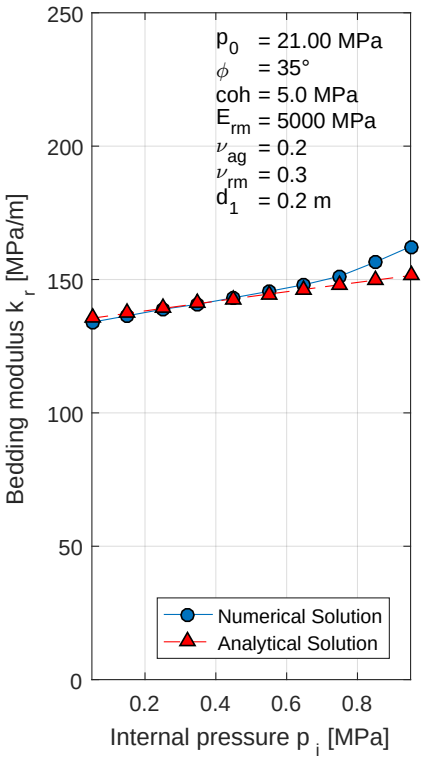

Figure 6.1: Application example - Comparison of the results.

7 Conclusion & Outlook

Aim of this thesis was the investigation of influencing parameters on the bedding modulus by means of numerical simulations and their incorporation in the state of the art calculation methodologies. However, the numerical results indicated significant discrepancies when compared to analytical solutions. A back-analysis of the theoretical rock mass influence depth d_2 of the "Extended approach" (Equation 2.13) provided negative values for d_2 and thus, demonstrated that the given approach cannot be applied for the determination of the bedding modulus without restrictions. Hence, an alternative calculation method, using familiar closed-form solutions, was presented. The main advantage of the presented method, compared to the conventional approach, is the incorporation of the strength properties of the subsoil and the primary stress state. This enables an improved description of the bedding modulus.

Nevertheless, the proposed closed-form solution is subject to simplifications. Since the method originates on the basic formulation $k_r = p_i/u_r$, a more appropriate description of the deformation behaviour should be sought. This should be realised for both layers, the rock mass and the backfill material. As an example, the equation according to Feder & Arwanitakis (1976) also includes a decreased shear strength of the rock mass within the plastic area as well as lateral pressure coefficients $K_0 \neq 1.0$. Concerning the backfill layer, future focus should be put on the incorporation of the stiffness moduli, which correspond to the respective loading conditions, in order to capture non-linear material behavior.

Bibliography

Behnen, G., Nevrly, T., & Fischer, O. (2013). Bettung von tunnelschalen, 235–282.

Duddeck, H. (1980). Empfehlungen zur berechnung von tunneln im lockergestein (recommendations for the design of tunnels in soil. *Die Bautechnik*, *57, Heft 10*, 349–356.

Duddeck, H. & Schulze, H. (1964). Spannungen in schildvorgetriebenen tunneln. *Beton- und Stahlbetonbau*, *59*(8), 169–175.

Feder, G. & Arwanitakis, M. (1976). Zur Gebirgsmechanik ausbruchsnaher Bereiche tiefliegender Hohlraumbauten. *Berg- und Huettenmaennische Monatshefte*, *121*.

Itasca Consulting Group Inc. (2017). *FLAC3D — Fast Lagrangian Analysis of Continua in Three-Dimensions, Ver.6.0*. Minneapolis: Itasca.

Lamé, G. (1852). *Leçons sur la théorie mathématique: de l'élasticité des corps solides*. Bachelier.

MathWorks Inc. (2017). *MATLAB: Version 9.3.0 (R2017b)*. Natick, Massachusetts: The MathWorks Inc.

Salençon, J. (1966). Expansion quasi-statique d'une cavitè a symètrie sphèrique ou cylindrique: Dans un milieu èlastoplastique. *Annales des Ponts et Chaussèes*, *III*, 175–187.

Salençon, J. (1969). Contraction quasi-statique d'une cavitè a symètrie sphèrique ou cylindrique: Dans un milieu èlastoplastique. *Annales des Ponts et Chaussees*, *139*(4), 231–236.

Seeber, G. (1999). *Druckstollen und Druckschächte: Bemessung - Konstruktion - Ausführung*. Stuttgart [u.a.]: Enke im Thieme-Verl.

Thienert, C. & Pulsfort, M. (2011). Segment design under consideration of the material used to fill the annular gap / tübbingbemessung unter berücksichtigung der eigenschaften des ringspaltmaterials. *Geomechanics and Tunnelling*, *4*(6), 665–680.

Windels, R. (1966). Spannungstheorie zweiter ordnung für den teilweise gebetteten kreisring. *Die Bautechnik*, *43*(8), 265–274.

Wissmann, W. (1968). Zur statischen berechnung beliebig geformter stollen und tunnelauskleidungen mit hilfe von stabwerkprogrammen. *Der Bauingenieur*, *43*(1), 1–8.